Electronic Supplementary Information for:

Insight into the Drastically Different Triplet Lifetimes of Bodipys by Optical/Magnetic Spectroscopies and Theoretical Computations

Zhijia Wang,[a]¶ *Antonio Toffoletti,*[b]¶ *Yuqi Hou,*[a] *Jianzhang Zhao,*[a,*] *Antonio Barbon*[b,*] *and Bernhard Dick*[c,*]

[a] State Key Laboratory of Fine Chemicals, School of Chemical Engineering, Dalian University of Technology, 2 Ling-Gong Road, Dalian 116024, P. R. China. E-mail: zhaojzh@dlut.edu.cn

[b] Dipartimento di Scienze Chimiche, Università degli Studi di Padova, Via Marzolo 1, 35131 Padova, Italy. E-mail: antonio.barbon@unipd.it

[c] Lehrstuhl für Physikalische Chemie, Institut für Physikalische und Theoretische Chemie, Universität Regensburg, Universitätsstr. 31, D-93053 Regensburg, Germany

E-mail: Bernhard.Dick@chemie.uni-regensburg.de

¶ These authors contributed equally to this work.

Contents

1. General Information of EPR model

In order to quantitatively study the ESP inversion kinetics of the compounds, we developed a model for the simulation of the TREPR spectra. A common triplet state for organic molecules is characterized by the presence of two interacting unpaired electrons residing on two different molecular orbitals. In zero magnetic field, its three non-degenerate substates are non-degenerate states because of the zero-field splitting interaction whose Hamiltonian can be expressed as Eq.1.

In photoexcited systems, the population of the triplet occurs mostly occurs through an intersystem crossing (ISC) process, like in the present case. The process leads to a selective population of the triplet sublevels from the singlet state[1] in a time scale which is much faster than the decay rate to the ground state. Under these conditions, an excitation obtained by a short laser flash produces an initial population **P** of the three sublevels which evolves in the dark according to the kinetic law.[2] Thus, not only a selective population of the triplet manifold is observed, but also a selective depopulation of the states, relaxing to the ground state.

$$\dot{\mathbf{P}}_{ZFS} = -\begin{vmatrix} k_x & 0 & 0 \\ 0 & k_y & 0 \\ 0 & 0 & k_z \end{vmatrix} \mathbf{P}_{ZFS} \qquad \text{(Eq. S1)}$$

TR-EPR measurements allows us to follow the dynamics of the three sublevels immersed in a magnetic field. In high field (HF), the triplet sublevels are mixed, and the three eigenstates of the system $|T_+>$, $|T_0>$, $|T_->$ are eigenfunctions of the Hamiltonian (expressed in the molecular frame, in the ZFS states base).[3]

$$H = \begin{vmatrix} -D_X & -ig_{eff}\mu_B B_Z & +ig_{eff}\mu_B B_Y \\ +ig_{eff}\mu_B B_Z & -D_Y & -ig_{eff}\mu_B B_X \\ -ig_{eff}\mu_B B_Y & +ig_{eff}\mu_B B_X & -D_Z \end{vmatrix} \qquad \text{(Eq.S2)}$$

where g_{eff} is combination of the principal values of the ***g***-tensor $g_{eff} = \sqrt{g_X^2 \sin^2\vartheta\cos^2\varphi + g_Y^2 \sin^2\vartheta\sin^2\varphi + g_Z^2 \cos^2\vartheta}$ and $D_{X,Y,Z}$ are the principal values of the D-tensor, that are related to the D and E values as: $D=3D_Z/2$ and $E=(D_X-D_Y)/2$, so that the HF eigenstates can be expressed as $|T_i> = c_i^x |T_x> + c_i^y |T_y> + c_i^z |T_z>$. The coefficients (eigenvectors) depend both on the strength of the magnetic field, but also on its orientation.

The time evolution of the population of the triplet sublevels $|T_+>$, $|T_0>$, $|T_->$ can be represented by an equation equivalent to Eq.1, where the decay rates k_x, k_y, k_z are substituted by unimolecular decay rates of each single high-field triplet sublevel k_+, k_0, k_-, that are related to the zero-field sublevels decay rates as $k_i = c_i^{x2}k_x + c_i^{y2}k_y + c_i^{z2}k_z$; c_i^j $(i = x, y, x \text{ and } j = +, 0, -)$.[4]

In the presence of spin relaxation, the complete time evolution of the system can be derived from ref.s [5,6], as

$$\dot{\mathbf{P}}_{HF} = -\begin{vmatrix} k_+ + (1-a_+)w & -(1-a_+)w & 0 \\ -(1-a_+)w & k_0 + (1-a_+)w & -(1+a_+)w \\ 0 & -(1+a_+)w & k_- + (1-a_+)w \end{vmatrix} \mathbf{P}_{HF} \qquad \text{(Eq. S3)}$$

$a_{+/-} \approx \Delta E_{+1,0/0,-1} / 2k_B T$. After a laser flash, the initial populations take into account the mixing of the ZFS states, thus[7]

$$p_i^0 = c_i^{x2} p_x^0 + c_i^{y2} p_y^0 + c_i^{z2} p_z^0 \qquad \text{(Eq. S4)}$$

The depopulation of the states is followed by TR-EPR, as the transition intensities depend on the population differences $\Delta P_{+/-}(\vartheta,\varphi,t) = P_{+/0}(\vartheta,\varphi,t) - P_{0/-}(\vartheta,\varphi,t)$ between the upper $|T_+>$ and the central $|T_0>$ state, or between the central and the lower $|T_->$ state. We note than, for each orientation of the magnetic field (ϑ,φ), the EPR transition can be in enhanced absorption or in emission and the states haven't a typical Boltzmann population.

In general, the data obtained by TR-EPR measurements are 3D surfaces extending over (or below) the time/field plane. They are rarely displayed in this form, rather it is preferred to show slices along the time (transients) or along the magnetic field (spectra) of these surfaces.[8]

One or the other representation is chosen if one wants 1) to highlight the presence of one or more high-spin states (typically triplet states) having different zero-field splittings, or to determine which particular route in the high state populates these species (appreciable in the spectra), or 2) one wants to follow the dynamics of the system (appreciable in the transients), that is the generation/decay of the population of the multiplet sublevels.

The full reconstruction of the 3D surface requires thus to follow in time the field-dependent lineshape and the intensity variation of the spectra as function of time.

The intensity variation of the spectra is due relaxation processes, either magnetic or optical processes.

2.0 Nanosecond Transient Absorption Spectra

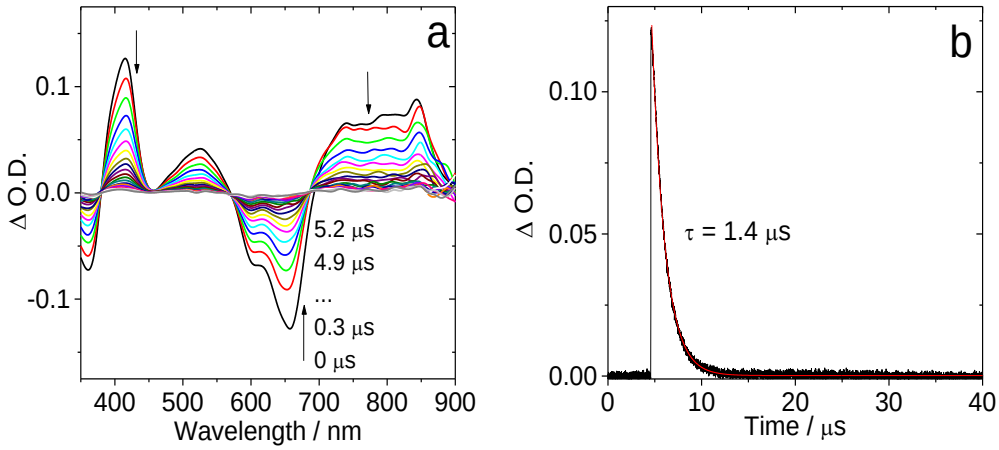

Figure S1. Nanosecond time resolved transient absorption spectra of **Nap-IBDP**. (a) **Nap-IBDP** upon ns pulsed laser excitation (λ_{ex} = 600 nm) and (b) decay trace of **Nap-IBDP** at 420 nm. $c = 1.0 \times 10^{-5}$ M in deaerated 2-Methyltetrahydrofuran, 293 K.

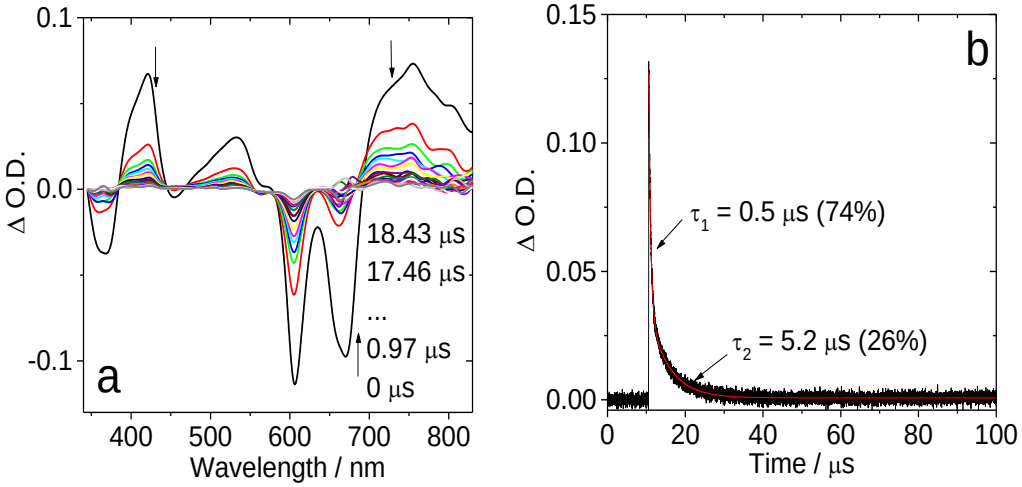

Figure S2. Nanosecond time resolved transient absorption spectra of **Nap-IBDP**. (a) **Nap-IBDP** upon ns pulsed laser excitation (λ_{ex} = 600 nm) and (b) decay trace of **Nap-IBDP** at 420 nm. $c = 1.0 \times 10^{-5}$ M in deaerated 2-Methyltetrahydrofuran, 78 K.

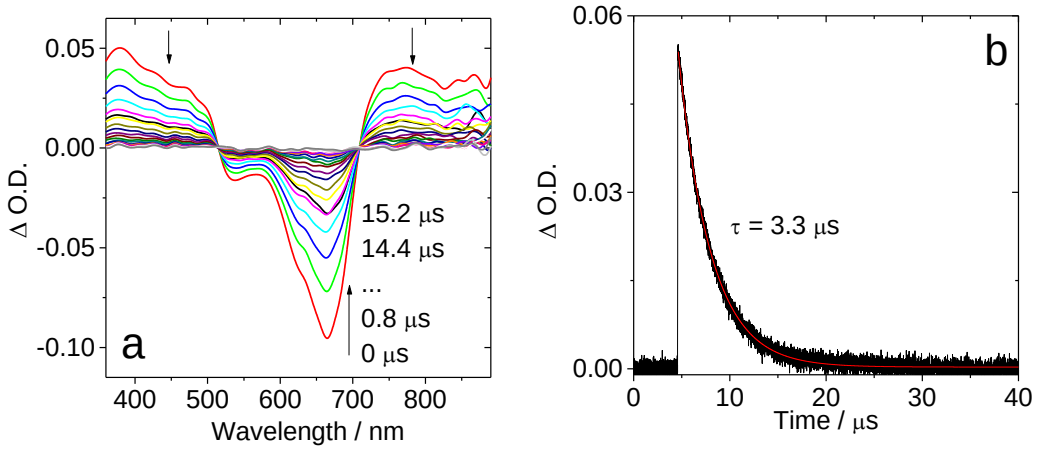

Figure S3. Nanosecond time resolved transient absorption spectra of **Aza-IBDP**. (a) **Aza-IBDP** upon ns pulsed laser excitation (λ_{ex} = 660 nm) and (b) decay trace of **Aza-IBDP** at 390 nm. $c = 1.0 \times 10^{-5}$ M in deaerated 2-Methyltetrahydrofuran, 293 K.

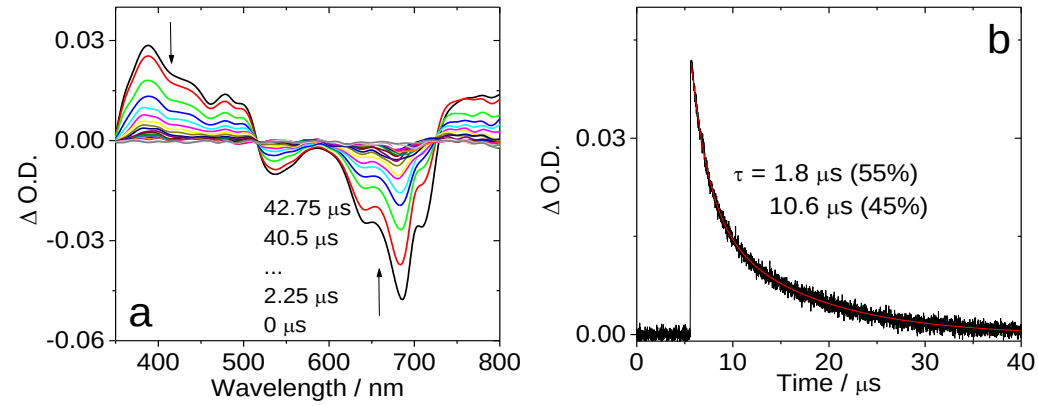

Figure S4. Nanosecond time resolved transient absorption spectra of **Aza-IBDP**. (a) **Aza-IBDP** upon ns pulsed laser excitation (λ_{ex} = 660 nm) and (b) decay trace of **Aza-IBDP** at 390 nm. $c = 1.0 \times 10^{-5}$ M in deaerated 2-Methyltetrahydrofuran, 78 K.

When the intrinsic lifetime of the triplet states is long and the concentration of the triplet states is large, triplet-triplet annihilation is an additional contribution to the decay of the transient absorption. The corresponding differential equation for the triplet concentration

$$\frac{dc_T}{dt} = -k_1 c_T - k_2 c_T^2 \qquad \text{(Eq. S5)}$$

has the solution

$$c_{\mathrm{T}}(t) = \frac{c_0 k_1}{\exp(k_1 t) \cdot (c_0 k_2 + k_1) - c_0 k_2} \qquad \text{(Eq. S6)}$$

Where c_0 is the initial triplet concentration. This leads to the following expression for the transient absorption

$$A(t) = \frac{\frac{A_0 \tau_2}{\tau_1}}{\exp\left(\frac{t}{\tau_1}\right) \cdot \left(1 + \frac{\tau_2}{\tau_1}\right) - 1} \qquad \text{(Eq. S7)}$$

Where A_0 is the initial transient absorption, $\tau_1 = 1/k_1$ is the intrinsic (unimolecular) lifetime of the triplet, and $\tau_2 = 1/c_0 k_2$. We fitted each data sets simultaneously by Eq. S7, with variation of all parameters (A_0, τ_2), but with the intrinsic triplet lifetime constrained to the same value in all data sets.

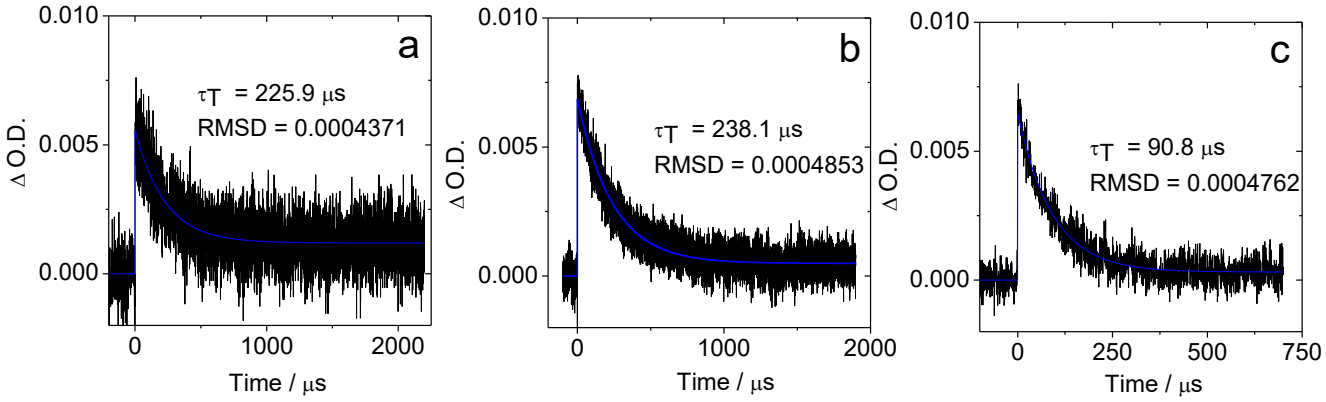

Figure S5. The decay traces of **IBDP** at 450 nm upon nanosecond pulsed laser excitation (λ_{ex} = 533 nm) in deaerated (a) 2-MeTHF (b) toluene and (c) acetonitrile. $c = 0.3 \times 10^{-6}$ M, recorded in the co-linear measurement mode of the LP980 ns-TA spectrometer. The decays are fitted with single monoexponential fit. The fitting result of the intrinsic triplet lifetime and the RMSD are shown in the figure.

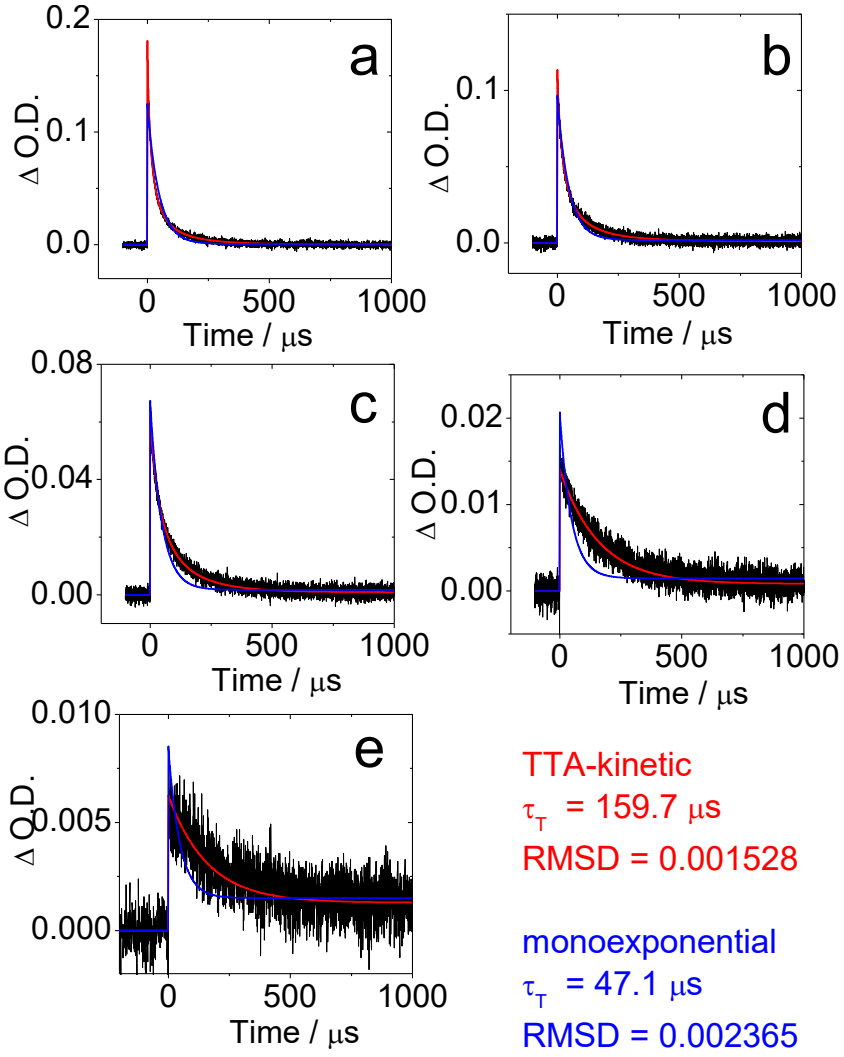

Figure S6. The decay traces of **IBDP** at 450 nm upon nanosecond pulsed laser excitation (λ_{ex} = 533 nm) in deaerated 2-MeTHF at different concentrations at 25 °C, recorded in the co-linear measurement mode of the LP980 ns-TA spectrometer. (a) $c = 2 \times 10^{-5}$ M, (b) $c = 1 \times 10^{-5}$ M, (c) $c = 5 \times 10^{-6}$ M, (d) $c = 1 \times 10^{-6}$ M and (e) $c = 0.3 \times 10^{-6}$ M. The decays are fitted with global fit with the TTA-kinetic model (in red color) and monoexponential fitting (in blue color), respectively. The fitting result of the intrinsic triplet lifetime and the RMSD are shown in the figure.

Table S1. Fitting parameters of Figure S6

	$\tau_1/\mu s$	A_0	$\tau_2/\mu s$
$c = 3.0 \times 10^{-7}$ M	160	0.005	∞ [a]
$c = 1.0 \times 10^{-6}$ M	160	0.013	∞ [a]
$c = 5.0 \times 10^{-6}$ M	160	0.062	56.3
$c = 1.0 \times 10^{-5}$ M	160	0.112	26.0
$c = 2.0 \times 10^{-5}$ M	160	0.181	15.3

[a] The fitted value was very large (i.e. many orders above the time window of the measurement). Hence the rate is essentially zero

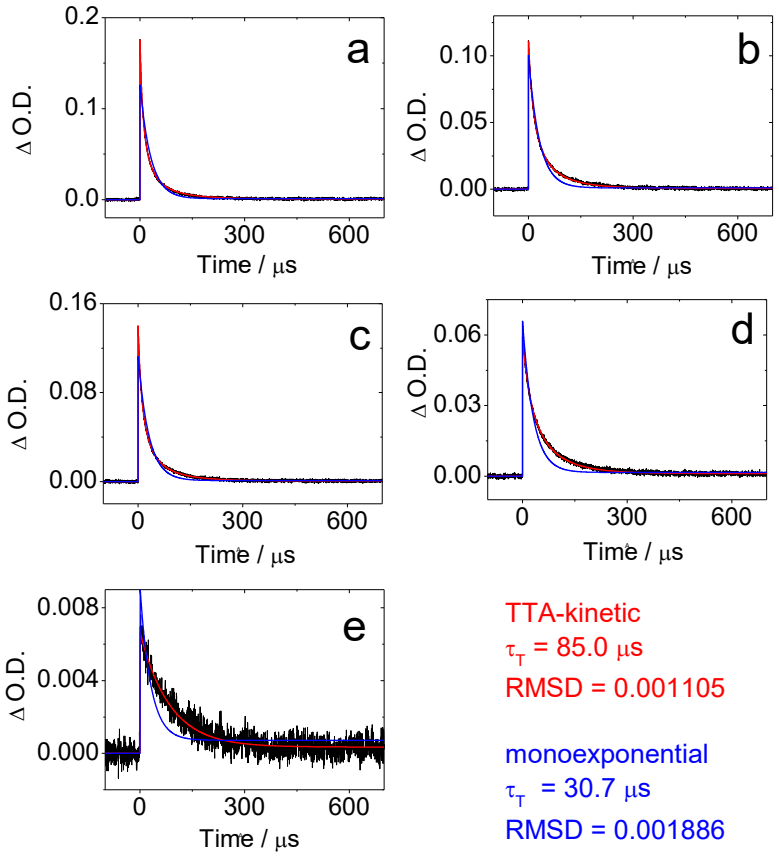

Figure S7. The decay traces of **IBDP** at 450 nm upon nanosecond pulsed laser excitation (λ_{ex} = 533 nm) in deaerated acetonitrile at different concentrations at 25 °C, recorded in the co-linear measurement mode of the LP980 ns-TA spectrometer. (a) $c = 2 \times 10^{-5}$ M, (b) $c = 1.5 \times 10^{-5}$ M, (c) $c = 1 \times 10^{-5}$ M, (d) $c = 5 \times 10^{-6}$ M and (e) $c = 0.3 \times 10^{-6}$ M. The decays are fitted with global fit with the TTA-kinetic model (in red color) and monoexponential fitting (in blue color), respectively. The fitting result of the intrinsic triplet lifetime and the RMSD are shown in the figure.

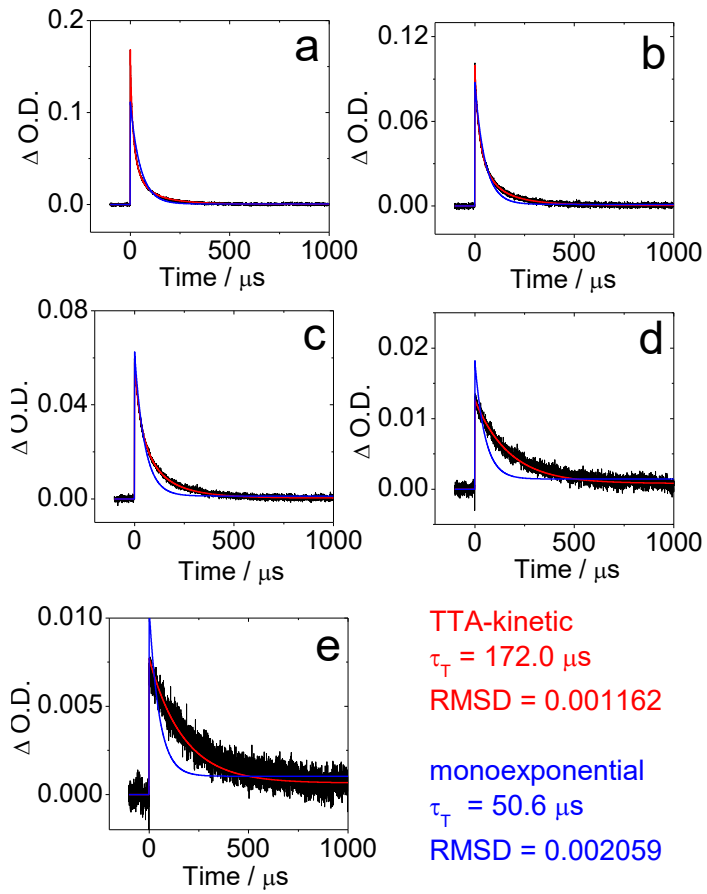

Figure S8. The decay traces of **IBDP** at 450 nm upon nanosecond pulsed laser excitation (λ_{ex} = 533 nm) in deaerated toluene at different concentrations at 25 °C, recorded in the co-linear measurement mode of the LP980 ns-TA spectrometer. (a) $c = 2 \times 10^{-5}$ M, (b) $c = 1 \times 10^{-5}$ M, (c) $c = 5 \times 10^{-6}$ M, (d) $c = 1 \times 10^{-6}$ M and (e) $c = 0.3 \times 10^{-6}$ M. The decays are fitted with global fit with the TTA-kinetic model (in red color) and monoexponential fitting (in blue color), respectively. The fitting result of the intrinsic triplet lifetime and the RMSD are shown in the figure.

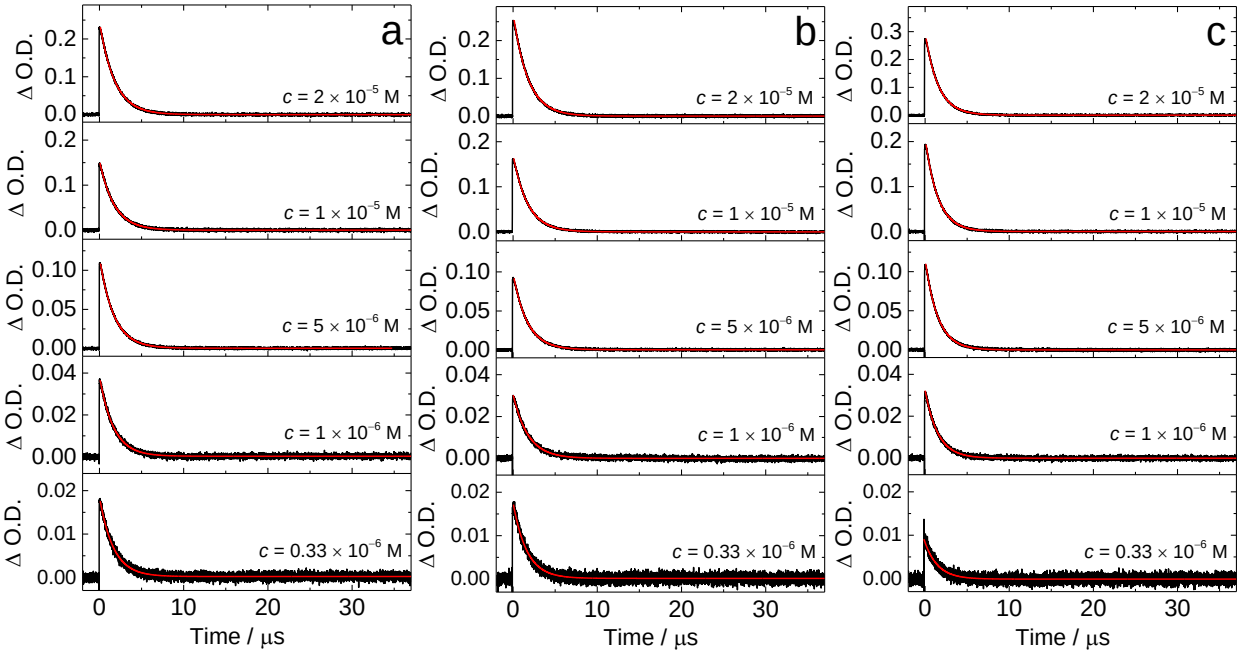

Figure S9. The decay traces of **Sty-IBDP** at 390 nm upon nanosecond pulsed laser excitation (λ_{ex} = 600 nm) in deaerated (a) toluene, (b) 2-methyltetrahydrofuran, and (c) acetonitrile at different concentration, recorded in the co-linear measurement mode of the LP980 ns-TA spectrometer. 25 °C.

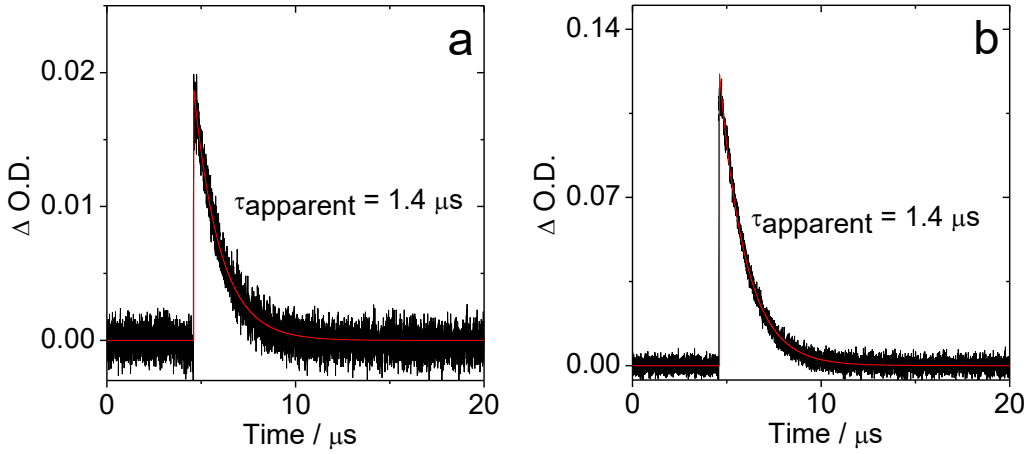

Figure S10. Triplet lifetimes of **Nap-IBDP** in deaerated 2-Methyltetrahydrofuran in different concentrations (a) c = 2.0 × 10^{-6} M (b) c = 2.0 × 10^{-5} M. The lifetimes are apparent triplet lifetimes. The intrinsic triplet lifetime is obtained by fitting of the decay traces with a kinetics model with triplet-triplet annihilation quenching effect considered (Table S2†).

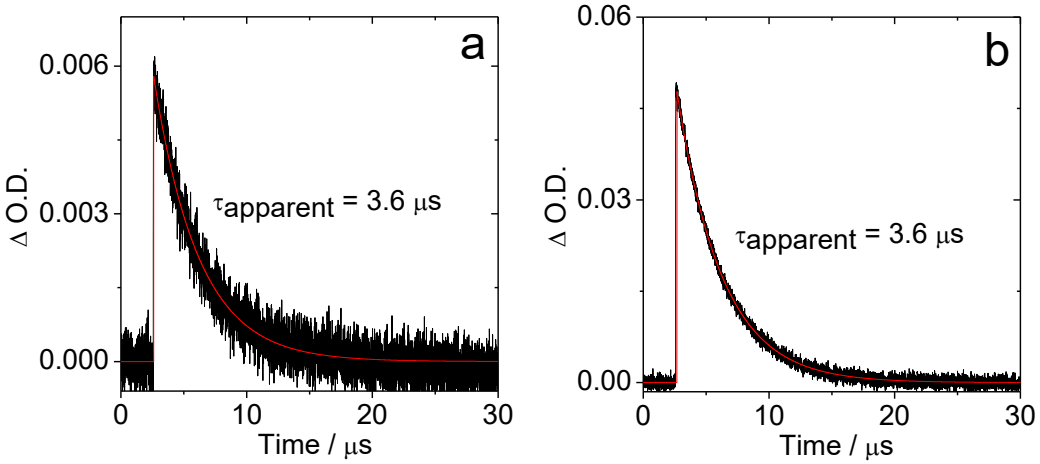

Figure S11. Triplet lifetimes of **Aza-IBDP** in deaerated 2-Methyltetrahydrofuran in different concentrations (a) $c = 2.0 \times 10^{-6}$ M (b) $c = 2.0 \times 10^{-5}$ M. The lifetimes are apparent triplet lifetimes. The intrinsic triplet lifetime is obtained by fitting of the decay traces with a kinetics model with triplet-triplet annihilation quenching effect considered (Table S2†).

Table S2. Fitting of the intrinsic triplet lifetimes of the compounds.

compound		$c = 2.0 \times 10^{-6}$ M		$c = 2.0 \times 10^{-5}$ M	
	τ_1/μs	A_0	τ_2/μs	A_0	τ_2/μs
Sty-IBDP	1.7	0.028	∞ [a]	0.1250	2358.0
Aza-IBDP	3.6	0.006	∞ [a]	0.04777	∞ [a]
Nap-IBDP	1.4	0.019	∞ [a]	0.1213	∞ [a]

[a] The fitted value was very large (i.e. many orders above the time window of the measurement). Hence the rate is essentially zero

Table S3. The apparent triplet lifetimes in Figure S6-S9.

Compounds	Concentration	$\tau_{apparent}$ / μs		
		TOL	2-MeTHF	ACN
IBDP	2×10^{-5} M	64	67	40
	1.5×10^{-5} M			48
	1×10^{-5} M	93	85	57
	5×10^{-6} M	126	123	70
	1×10^{-6} M	224	215	
	0.3×10^{-6} M	239	225	90
Sty-IBDP	2×10^{-5} M	1.8	1.8	1.5
	1×10^{-5} M	1.7	1.7	1.5
	5×10^{-6} M	1.7	1.7	1.5
	1×10^{-6} M	1.7	1.8	1.5
	0.3×10^{-6} M	1.6	1.6	1.5

Analysis of the TTA self-quenching constant k_2

The self-quenching (due to the TTA effect) was considered in the kinetic model. The self-quenching constant can be estimated according to

$$\frac{1}{\tau_2} = c_0 k_2 \qquad \text{Eq. S8}$$

$$A = c_0 \epsilon_T d \qquad \text{Eq. S9}$$

where the c_0 is the initial triplet concentration, k_2 is the self-quenching constant, i.e., TTA rate constant. ϵ_T is the extinction coefficient of the triplet at 450 nm, d is the light path. The above fitting in Figure S6 yields the amplitudes A (the ΔO.D. value of the decay in each concentration) and the effective time constant τ_2 (Table S1).

According to Eq. S8 and Eq. S9, $1/\tau_2$ should increase linearly with A, and the slope a of this plot should be

$$a = \frac{c_0 k_2}{c_0 \epsilon_T d} = \frac{k_2}{\epsilon_T d} \qquad \text{Eq. S10}$$

Hence

$$k_2 = a\, \epsilon_T d \qquad \text{Eq. S11}$$

The ϵ_T is estimated (see Table S4) from Figure 2c in the manuscript, according to $\Delta A_S/\varepsilon_S = A/\varepsilon_T$, where ΔA_S is the initial ΔO.D. value of bleaching band, ε_S is the molar extinction coefficient of singlet bleaching band.

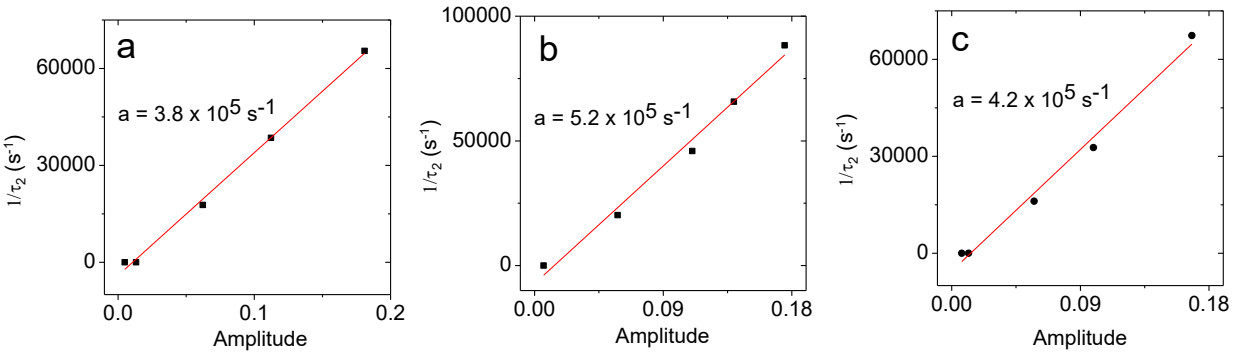

Figure S12. Fitting results of the decay traces of **IBDP** (a) in 2-MeTHF, (b) in acetonitrile and (c) in toluene.

Table S4. Calculation of the ε_T of the **IBDP**: [a]

	$c = 2\times 10^{-5}$ M
ΔA_S	0.197
ε_S / $M^{-1}cm^{-1}$	8.55×10^4
A	0.044
ε_T / $M^{-1}cm^{-1}$	1.9×10^4

Table S5. Estimation of the self-quenching constant k_2 of the **IBDP**: [a]

	2-MeTHF	acetonitrile	toluene
a / s^{-1}	3.8×10^5	5.2×10^5	4.2×10^5
k_2 / $M^{-1}s^{-1}$	7.2×10^9	1.0×10^{10}	8.0×10^9

The slope a are fitted (Figure S12) to be 3.8×10^5 s^{-1}, 5.2×10^5 s^{-1} and 4.2×10^5 s^{-1} in 2-MeTHF, acetonitrile and toluene, respectively. We use an estimated value 1 cm for d, as the decay curves are recorded in the co-linear measurement mode of the LP980 ns-TA spectrometer. Hence the self-quenching constant are estimated to be 7.2×10^9 $M^{-1}s^{-1}$, 1.0×10^{10} $M^{-1}s^{-1}$ and 8.0×10^9 $M^{-1}s^{-1}$ in 2-MeTHF, acetonitrile and toluene, respectively. It should be noted that the values are overestimated to an extent as the d value should be smaller than 1 cm.

For the three other compounds, the best fit resulted in very large values for $\tau_2 = 1/(k_2 * c_0)$. Here k_2 is the bimolecular rate constant, and c_0 is the initial triplet concentration. Obviously then, $k_2 \approx 0$ in these cases, i.e., TTA can not compete with unimolecular decay. So the short triplet lifetime is intrinsic.

3.0 Time-resolved EPR Spectra

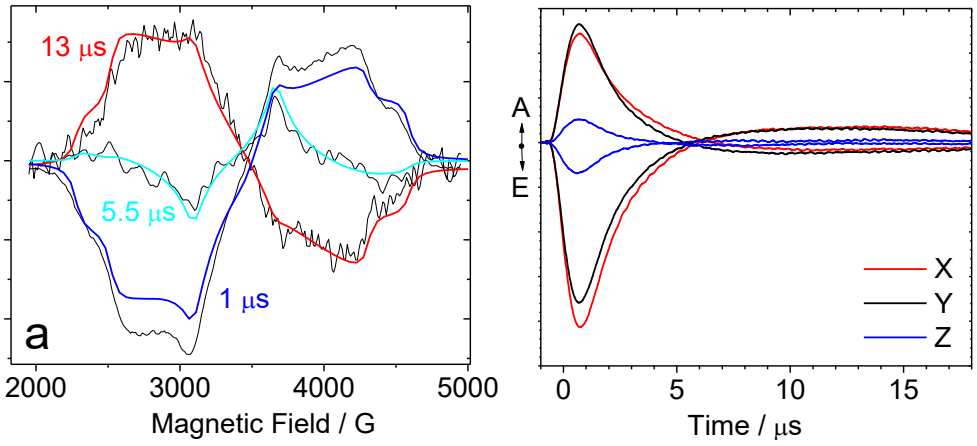

Figure S13. (a) Time-resolved spectra taken at different time delays of a frozen solution of **Aza-IBDP** in toluene/Me-THF (3:1, v/v), $c = 3.0 \times 10^{-5}$ M, excited at 650 nm (2 mJ/shot). (b) Transient signals taken at magnetic field positions of resonance of the principal components.

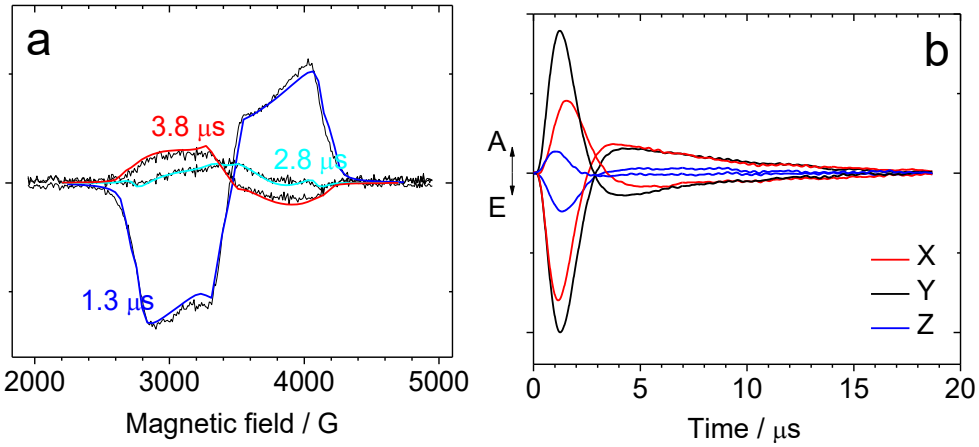

Figure S14. (a) Time-resolved spectra taken at different time delays of a frozen solution of **Nap-IBDP** in toluene/ Me-THF (3:1), $c = 3.0 \times 10^{-5}$ M, excited at 547 nm (2 mJ/shot). (b) Transient signals taken at magnetic field positions of resonance of the principal components.

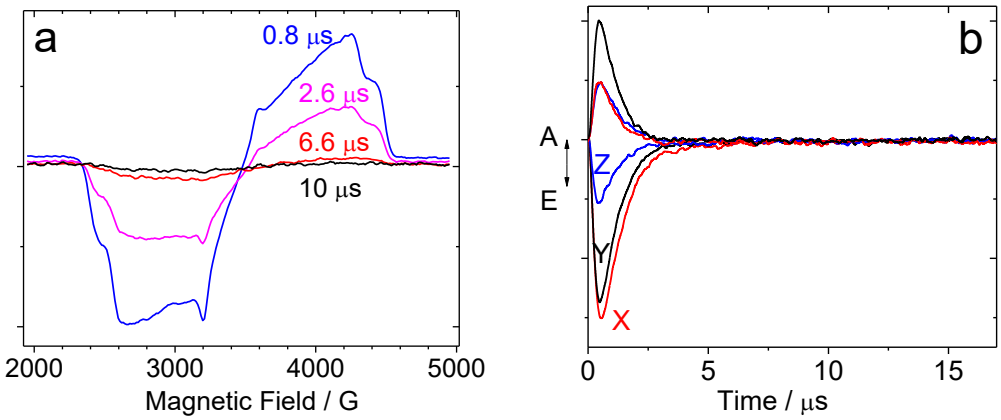

Figure S15. (a) Time-resolved spectra taken at different time delays of a frozen solution of **IBDP** in toluene/Me-THF (3:1), c = 3.0 × 10^{-5} M, excited at 532 nm (3 mJ/shot). (b) Transient signals taken at magnetic field positions of resonance of the principal components.

4. Computation Study

Table S6. Experimental and calculated ZFS principal values (X, Y and Z) obtained with different methods [a]

	Exp	CAS-CI C_2-sym	CAS-CI C_1-sym	DFT (BP86) C_2-sym	DFT (BP86) C_1-sym
IBDP	–330	–487 [b]		–456 [b]	
	–1630	–972		–697	
	1960	1459		1152	
Sty-IBDP	–140	–89	–88	–141	–145
	–1232	–700	–696	–359	–352
	1372	789	784	498	500
Nap-IBDP	–204	63	30	–40	–66
	–1243	567	608	–310	–321
	1447	–630	–638	350	387
Aza-IBDP [c]	–518	–214	–195	–289	–300
	–1649	–645	–680	–323	–448
	2167	859	874	612	748

[a] Units are MHz. Unrestricted DFT optimization of the geometry of the lowest triplet state found two minima, with C_1 and C_2-symmetry, which are very close in energy (ca. 1 kcal/mole). These calculations yield also ZFS parameters. CAS-CI at these geometries used 10 electrons in an active space of 10 molecular orbitals from a RHF calculation. For **Nap-IBDP** we preserved the labeling according to the sign of the two largest values. [b] This is for C_{2v} geometry. [c] For this molecule the principal direction of the X and Y result swap in the calculations, the reason is not clear, yet.

The calculation show that the molecular orbitals are rather sensitive to the geometry of the molecule. Table S6 shows that the simulation of the ZFS conducted with CAS (and DFT) methods reasonably reproduced the trend of experimental values but is not satisfactory. ZFS are parameters that are very sensitive to frontier orbitals;[9] therefore, it is rather difficult to have a good reproduction of the experimental value, in particular when conformational movements of the molecules can modulate the extension of the delocalization.

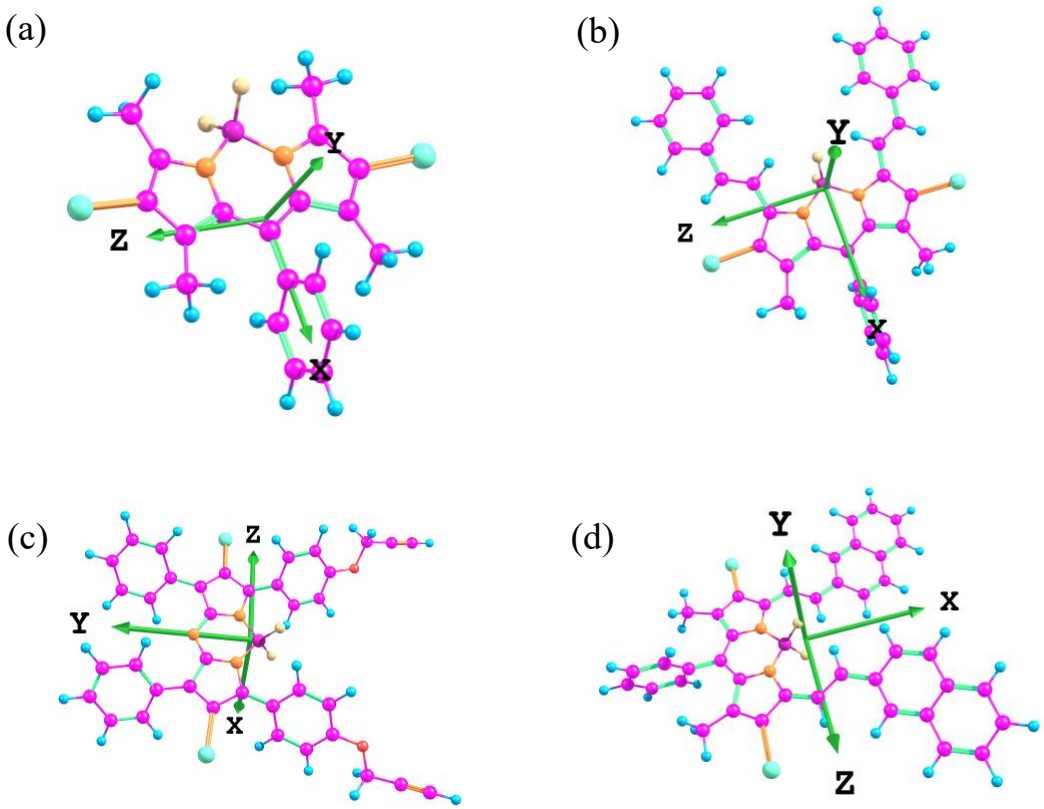

Figure S16. The orientation of the ZFS axes (from the DFT calculations) for the most stable conformer of (a) **IBDP** (b) **Sty-IBDP** (c) **Aza-IBDP** (d) **Nap-IBDP**. Z is always the long axis of the Bodipy chromophore.

Table S7. Symmetry and SOC matrix elements [a] for optimized triplet geometries in their ZFS coordinate system.

		S_1/T_1		
Molecule	Symmetry	x	y	z
IBDP	C_{2v}	0.00	0.00	0.00
Sty-IBDP	C_1	0.14	–0.02	0.47
	C_2	3.69	0.00	0.00
Aza-IBDP	C_2	0.27	–13.43	0.05
	C_1	–1.88	2.72	–32.12
Nap-IBDP	C_2	0.02	0.00	0.00
	C_1	–0.52	0.31	2.14
IBDP-H [b]	C_{2v}	0.00	0.00	0.00
Sty-IBDP-H [b]	C_1	0.00	0.00	–0.08
	C_2	0.06	0.00	0.00
Aza-IBDP-H [b]	C_2	0.00	0.04	0.00
	C_1	0.04	0.06	–0.05
Nap-IBDP-H [b]	C_2	–0.02	0.00	0.00
	C_1	0.03	0.04	0.09

[a] In cm^{-1} units. [b] The addition of -H means that in the corresponding structures of Scheme 2, Iodine atoms where substituted by hydrogen atoms. In kcal/mole units. CAS(10|10)-CI with the molecular orbitals from a RHF calculation at the triplet geometry optimized with BP86 functional.

5.0 Molecular dynamic (MD) simulation of IBDP

We performed, for each molecule, a MD calculation with 2000 timesteps of 1 fs (i.e. 2000 DFT calculations of energy and gradient) and extracted a snapshot every 100 fs. This was done with the same DFT method that was used to calculate the ground state structures. In a second step, the snapshots were aligned so that they most closely matched the original structure, thus removing translation and rotation that can occur in the MD calculation. Finally, at these 20 snapshot geometries the RHF orbitals were calculated with the DKH Hamiltonian and the DK-cc-pVTZ basis (which includes all inner electrons of Iodine). These SCF-orbitals were used in a CAS-CI(10|10) to find the lowest singlet and triplet states. Between these states the SOC-ME were calculated.

A transition between a singlet and a triplet state is enabled by SOC, and the rate constant is proportional to the square of the SOC-ME:

$$k = A\left(H_x^2 + H_y^2 + H_z^2\right) = A\,\mathrm{H}^2 \qquad \text{Eq. S12}$$

Then we averaged H^2 for the 20 snapshots. The effective SOC-ME then is

$$H = \sqrt{\langle H_x^2 + H_y^2 + H_z^2 \rangle} \qquad \text{Eq. S13}$$

I.e., a rigid system with that SOC-ME will show the same rate as the averaged ensemble.

The square root of this average is 4.9 cm^{-1} for the S_1/T_1 coupling and can be considered as an effective vibrationally induced SOC-ME.

6.0 Emission Spectra at 298 K and 80 K

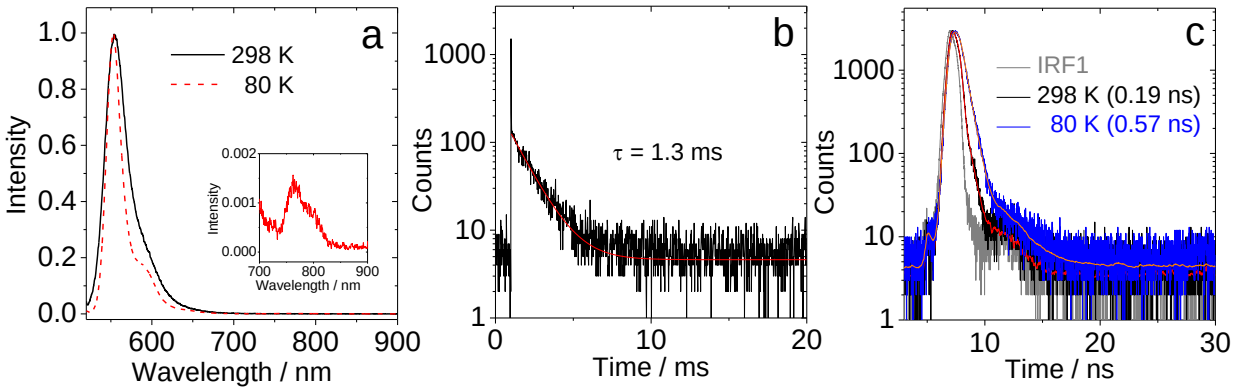

Figure S17. (a) The emission spectra of **IBDP** at 298 K and 80 K, and the inset shows the phosphorescence spectrum at 80 K. (b) The phosphorescence lifetime detected at 757 nm at 80 K. (c) The emission lifetimes detected at 550 nm. In deaerated 2-methyltetrahydrofuran solution, $c = 1 \times 10^{-5}$ M, $\lambda_{ex} = 510$ nm.

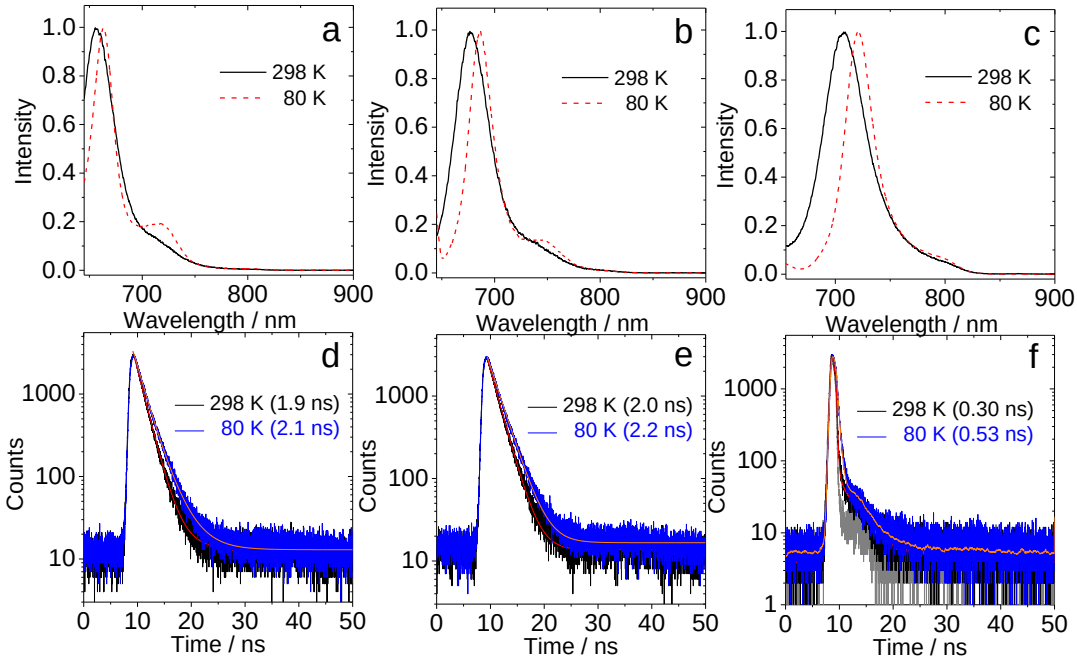

Figure S18. The emission spectra and their relative decay curves at 298 K and 80 K of (a, d) **Sty-IBDP** detected at 657 nm, (b, e) **Nap-IBDP** detected at 680 nm, and (c, f) **Aza-IBDP** detected at 712 nm. In deaerated 2-methyltetrahydrofuran solution, $c = 1 \times 10^{-5}$ M, λ_{ex} = 635 nm.

7. Molecular Structure Characterization Data

The synthesis of **IBDP** was according to literature.[10] ^{1}H NMR (400 MHz, $CDCl_3$): δ = 7.53–7.52 (m, 3H), 7.26–7.24 (m, 2H), 2.65 (s, 6H), 1.39 (s, 6H).

The synthesis of **Sty-IBDP** was according to literature.[11] ^{1}H NMR (400 MHz, $CDCl_3$): δ = 8.18 (d, 2H, J = 16.0 Hz), 7.73 (s, 1H), 7.69–7.66 (m, 5H), 7.55–7.54 (m, 3H), 7.43 (t, 4H, J = 8.0 Hz), 7.37 (d, 2H, J = 8.0 Hz), 7.31–7.29 (m,2H), 1.46 (s, 6H).

The synthesis of **Nap-IBDP** was according to literature.[11] ^{1}H NMR (400 MHz, $CDCl_3$): δ = 8.38 (s, 1H), 8.34 (s, 1H), 8.01 (s, 2H), 7.90–7.84 (m, 10H), 7.56–7.55 (m, 3H), 7.51–7.49 (m, 4H), 7.33–7.31 (m, 2H), 1.48 (s, 6H).

8. ^{1}H-NMR Spectra

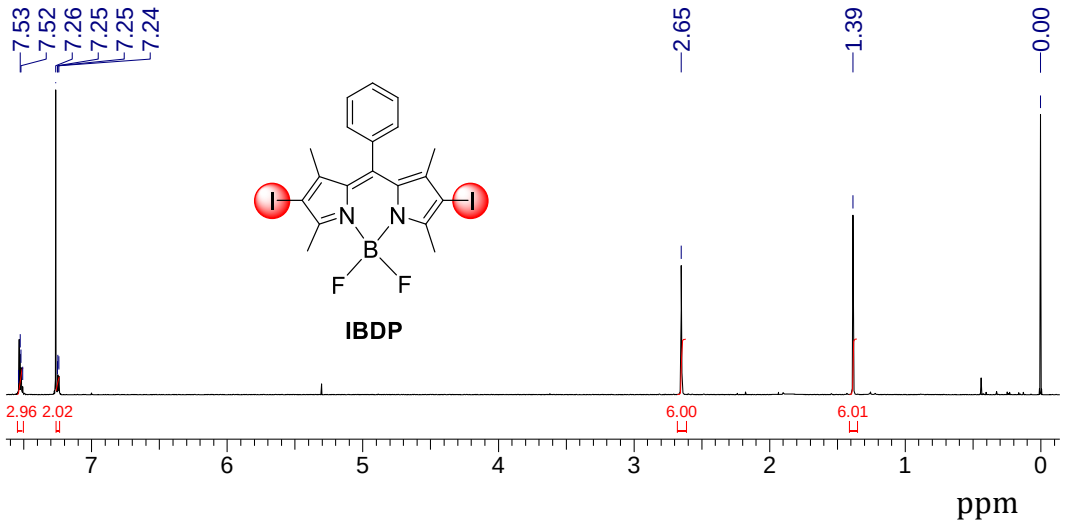

Figure S19. ^{1}H NMR of compound **IBDP** in $CDCl_3$ (400 MHz), 25°C.

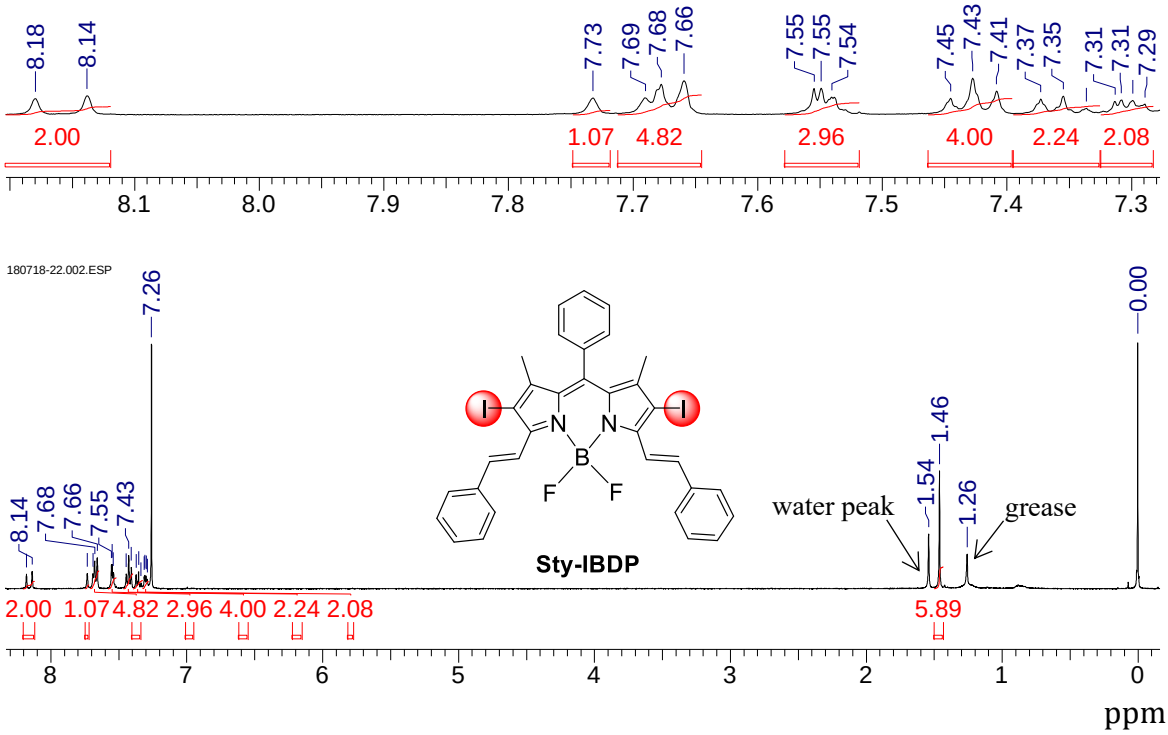

Figure S20. ^{1}H NMR spectrum of compound **Sty-IBDP** in $CDCl_3$ (400 MHz), 25°C.

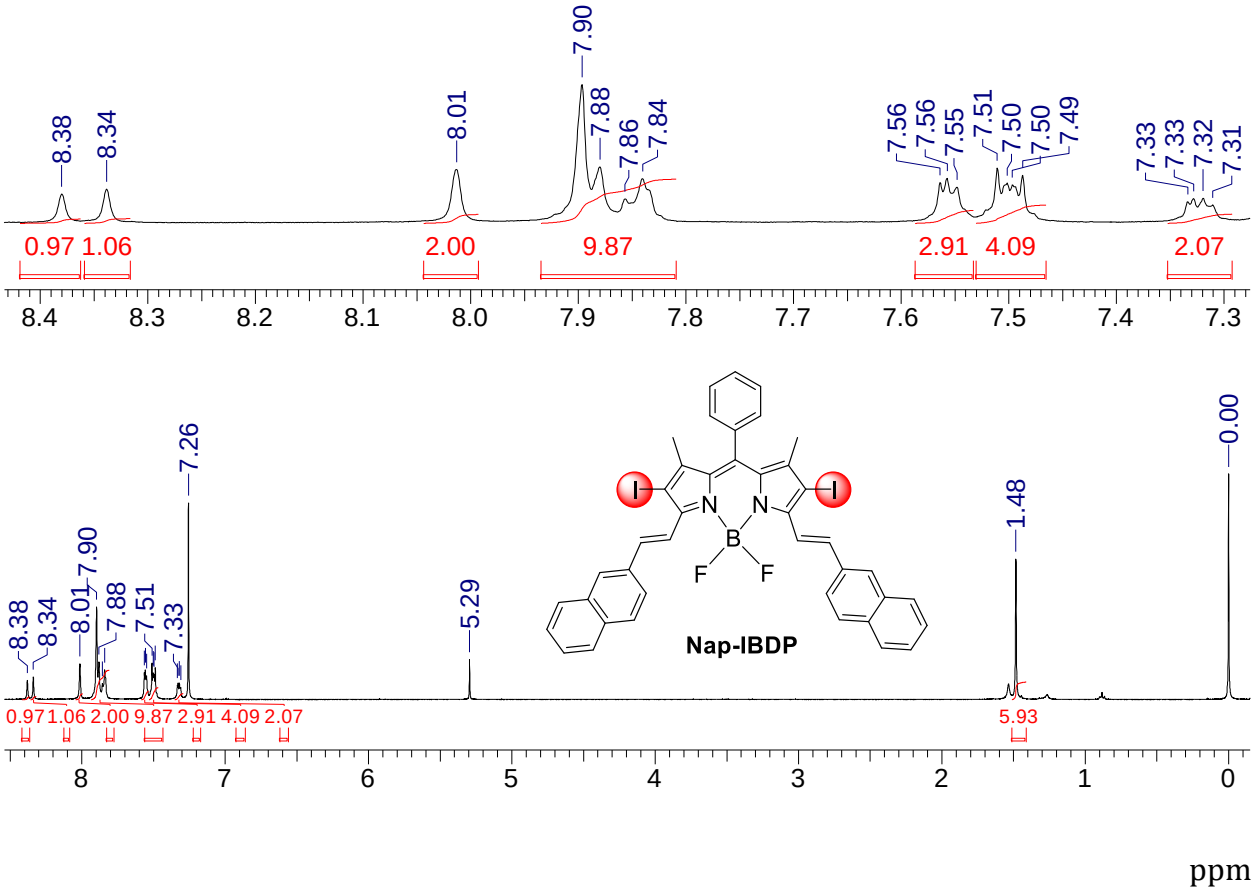

Figure S21. ^{1}H NMR of compound **Nap-IBDP** in $CDCl_3$ (400 MHz), 25°C.

9. References

1. A. Toffoletti, Z. Wang, J. Zhao, M. Tommasini, A. Barbon. Precise determination of the orientation of the transition dipole moment in a Bodipy derivative by analysis of the magnetophotoselection effect. *Phys. Chem. Chem. Phys.*, 2018, **20**, 20497–20503.

2. R. H. Clarke, R. H. Hofeldt. Optically detected zero field magnetic resonance studies of the photoexcited triplet states of chlorophyll a and b. *J. Chem. Phys.*, 1974, **61**, 4582–4587.

3. J. A. Weil, J. R. Bolton Electron Paramagnetic Resonance. Elementary Theory and Practical Applications, Wiley (2007).

4. C. Corvaja, L. Franco, K. M. Salikhov, V. K. Voronkova. The first observation of electron spin polarization in the excited triplet states caused by the triplet-triplet annihilation. *Appl. Magn. Reson.*, 2005, **28**, 181–193.

5. C.J. Winscom Z. Analysis of Spin Polarisation Transients in Periodically Photo-excited Triplet States. *Z. Naturforsch. A.*, 1975, **30**, 571–582.

6. H. Levanon, S. Vega. Analysis of the transient EPR signals in the photoexcited triplet state. Application to porphyrin molecules. *J. Phys. Chem.*, 1974, **61**, 2265–2274.

7. O.Gonen, H. Levanon. Time-resolved EPR spectroscopy of electron spin polarized ZnTPP triplets oriented in a liquid crystal. *J. Phys. Chem.*, 1985, **89**, 1637–1643.

8. M. Di Valentin, S. Ceola, G. Agostini, G. M. Giacometti, A. Angerhofer, O. Crescenzi, V. Barone, D. Pulse ENDOR and density functional theory on the peridinin triplet state involved in the photo-protective mechanism in the peridinin–chlorophyll a–protein from Amphidinium carterae. *BBA-Bioenergetics*, 2008, **1777**, 295–307.

9. A. Barbon, M. G. D. Farra, S. Ciuti, M. Albertini, L. Bolzonello, L. Orian, M. D. Valentin. Comprehensive investigation of the triplet state electronic structure of free-base 5,10,15,20-tetrakis(4-sulfonatophenyl)porphyrin by a combined advanced EPR and theoretical approach. *J. Chem. Phys.*, 2020, **152**, 034201.

10. C. Zhang, J. Zhao, S. Wu, Z. Wang, W. Wu, J. Ma, S. Guo, L. Huang. Intramolecular RET Enhanced Visible Light-Absorbing Bodipy Organic Triplet Photosensitizers and Application in Photooxidation and Triplet–Triplet Annihilation Upconversion. *J. Am. Chem. Soc.*, 2013, **135**, 10566–10578.

11. L. Huang, J. Zhao, S. Guo, C. Zhang, J. Ma. Bodipy Derivatives as Organic Triplet Photosensitizers for Aerobic Photoorganocatalytic Oxidative Coupling of Amines and Photooxidation of Dihydroxylnaphthalenes. *J. Org. Chem.*, 2013, **78**, 5627–5637.